

1 **Assessment of retrieved GMI emissivity over land, snow, and sea ice in the**  
2 **GEOS system**

3  
4 Bryan Mills Karpowicz,<sup>a,b,c</sup> Yanqiu Zhu,<sup>a,b</sup> Stephen Joseph Munchak,<sup>c</sup> Will McCarty<sup>a</sup>

5 <sup>a</sup> *Global Modeling and Assimilation Office, Goddard Space Flight Center, Greenbelt, MD*

6 <sup>b</sup> *Goddard Earth Sciences and Technology and Research, Greenbelt, MD*

7 <sup>c</sup> *University of Maryland Baltimore County, Baltimore, MD*

8 <sup>c</sup> *Mesoscale Atmospheric Processes Laboratory, Goddard Space Flight Center, Greenbelt, MD*

9  
10  
11 *Corresponding author: Author Name, [bryan.m.karpowicz@nasa.gov](mailto:bryan.m.karpowicz@nasa.gov)*  
12

## ABSTRACT

13  
14  
15  
16  
17  
18  
19  
20  
21  
22  
23  
24  
25  
26  
27  
28  
29  
30  
31  
32

Directly assimilating microwave radiances over land, snow and sea ice remains a significant challenge for data assimilation systems. These data assimilation systems are critical to the success of global numerical weather prediction systems including the Global Earth Observing System-Atmospheric Data Assimilation System (GEOS-ADAS). Extending more surface sensitive microwave channels over land, snow and ice could provide a needed source of data for Numerical Weather Prediction particularly in the Planetary Boundary Layer (PBL). Unfortunately, the accuracy of emissivity models currently available within the GEOS-ADAS along with other data assimilation systems are insufficient to simulate and assimilate radiances. Recently, Munchak et al. (2020) published a 5-year climatological database for retrieved microwave emissivity from the GPM Microwave Imager (GMI) aboard the Global Precipitation Measurement (GPM) Mission. In this work the database is utilized by modifying the GEOS-ADAS to use this emissivity database in place of the default emissivity value available in the Community Radiative Transfer Model (CRTM), which is the fast radiative transfer model used by the GEOS-ADAS. As a first step, the GEOS-ADAS is run in a so-called “stand-alone” mode to simulate radiances from GMI using the default CRTM emissivity, and replacing the default CRTM emissivity models with values from Munchak et al, 2020. The simulated GMI observations using Munchak et al., 2020 agree more closely with observations from GMI. These results are presented along with a discussion of the implication for GMI observations within the GEOS-ADAS.

### 1. Introduction

33  
34  
35  
36  
37  
38  
39  
40  
41  
42  
43  
44

Measurements from microwave sounders and imagers provide a valuable source of information including atmospheric temperature and water vapor in Numerical Weather Prediction (NWP) systems that assimilate these observations directly over water surfaces (oceans and other large water bodies). In a recent decadal survey, targeted observables in the Planetary Boundary Layer (PBL) were cited as a key need for future observations (NASSEM, 2018). Microwave instruments which sense in the PBL are currently available, however, utilizing surface-sensitive microwave observations for atmospheric data assimilation remains a challenge over land, snow and sea ice. This is in part due to the inability of surface emissivity models used by NWP data assimilation systems to simulate observations with sufficient accuracy. The GEOS-ADAS (Todling and el Akkraoui, 2018) which utilizes the Community Radiative Transfer Model (CRTM) (Han, 2006; Chen 2009) is no exception.

45 The ECMWF system has retrieved instantaneous surface emissivity from surface-sensitive  
46 channels for SSMI/S and MHS radiance observations, and applies these estimates to the  
47 closest channels higher in frequency (Baordo and Geer 2016) in the calculation of simulated  
48 radiances. This approach currently is also being tested in the GEOS-ADAS for AMSU-A and  
49 ATMS radiances (Zhu et al. 2021). No or minimal emissivity spectral variability has been  
50 assumed in the above-mentioned studies. This is generally supported by retrievals in  
51 Munchak et al., 2020 where the spectral variability was nominally 0.03 between 89-166 GHz  
52 except over shallow snow cover . Recently, work by Munchak et al., 2020 (hereby referred to  
53 as M2020) provided a new database for emissivity over land, snow and sea ice retrieved from  
54 the NASA Global Precipitation Measurement (GPM) Mission. Compared with Tool to  
55 Estimate Land Surface Emissivities at Microwave (TELSEM<sup>2</sup>; Wang et al., 2017), M2020  
56 provides emissivities for more frequencies (i.e., 10.7 GHz V/H). Moreover, this database is  
57 unique in that it utilizes both active and passive data to retrieve surface emissivity and  
58 normalized radar cross section. While the emissivity values may be useful for other sensors,  
59 they are most applicable to the GPM Microwave Imager (GMI). In this work the GEOS-  
60 ADAS is modified to utilize emissivity values from Munchak et al, 2020 in place of values  
61 used by CRTM. Presently, only GMI radiances over ocean are used in the operational GEOS-  
62 ADAS. This study will focus on the GMI radiances over land, snow, and ice, as a first  
63 attempt to evaluate GMI radiances over these non-water surface types. Two cases are then  
64 presented, one with one week of observation minus background departures using the  
65 modified GEOS-ADAS, and one utilizing the original GEOS-ADAS. It should be noted that  
66 the surface emissivity models in CRTM are not state of the art and are scheduled to be  
67 replaced by the Community Surface Emissivity Module (CSEM; Chen and Weng, 2016).  
68 Simulations using default CRTM emissivity values are used merely as reference comparing  
69 against M2020, and is not a thorough comparison against other more state of the art modules  
70 such as CSEM. This paper is organized as follows: First, in Section 2 the microwave  
71 emissivity databases and models used are discussed, next, in Section 3 an evaluation of  
72 observation minus background values produced by the GEOS-ADAS are presented. Finally,  
73 the implications for assimilating GMI surface sensitive channels and the potential benefits in  
74 NWP including better representation of the PBL are discussed.

## 75 **2. Microwave Surface Emissivity Databases and Models**

76 There has been significant progress made in the last few years with respect to microwave  
77 emissivity databases. Some recently developed packages include TELSEM<sup>2</sup> and CSEM

78 (Chen and Weng, 2016). TELSEM<sup>2</sup> is currently distributed with RTTOV (Saunders et al.,  
79 2020), while CSEM will soon be included with CRTM. The surface models (land, snow and  
80 ice) currently available in the CRTM are the physical model LandEm (Weng et al.,2001) for  
81 land surfaces, LandEm or an empirical/semi-empirical models for specific sensors over snow  
82 covered surfaces, or empirical/semi-empirical model for specific sensors over ice surfaces. A  
83 database designed specifically for GMI has been recently made available in M2020. This  
84 database is unique in that it uses active microwave data from the Dual-frequency  
85 Precipitation Radar (DPR) on GPM, along with passive microwave data from GMI. The  
86 details of both M2020 and emissivity models present in the CRTM’s default configuration  
87 which are relevant to GMI are discussed.

88 *a. Emissivity Available in CRTM*

89 The control case in this work utilizes the default emissivity models over land, snow, and sea  
90 ice available for GMI in the CRTM. As mentioned previously, the emissivity models utilized  
91 by the CRTM are sensor specific, however, in the case of GMI there are no derived empirical  
92 or semi-empirical models for snow or sea ice. The LandEm physical model provides  
93 emissivity values for frequencies below 80 GHz over land and snow-covered surfaces.  
94 LandEm is a physical model derived from a 3-layer radiative transfer model along with  
95 modified Fresnel equations at layer interfaces. The model uses several parameterizations, and  
96 variables obtained from the GEOS system such as Leaf Area Index (LAI), snow depth,  
97 surface type, along with sensor view geometry parameters such as zenith angle. It was  
98 validated with available data at the time from ground-based measurements (Mätzler, 1994),  
99 and satellite data from AMSU-A. For frequencies above 80 GHz, the CRTM will use a  
100 constant value of 0.95 for land, and 0.9 for snow. Given there is no empirical model for sea  
101 ice available in the case of GMI, the CRTM will use a default value of 0.92. For convenience,  
102 the source of emissivity values for each GMI channel are summarized in Table 1. The  
103 nomenclature “V” refers to vertical polarization, while “H” refers to horizontal polarization.

104 Table 1: The source of emissivity used by the CRTM for each surface type and GMI Channel

Surface	10.6 GHz V	10.6 GHz H	18.7 GHz V	18.7 GHz H	23 GHz V	37 GHz V	37 GHz H	89 GHz V	89 GHz H	166 GHz V	166 GHz H	183 V +/- 3 GHz	183 V +/- 7 GHz
Land	LandEm	LandEm	LandEm	LandEm	LandEm	LandEm	LandEm	0.95	0.95	0.95	0.95	0.95	0.95
Snow	LandEm	LandEm	LandEm	LandEm	LandEm	LandEm	LandEm	0.9	0.9	0.9	0.9	0.9	0.9
Ice	0.92	0.92	0.92	0.92	0.92	0.92	0.92	0.92	0.92	0.92	0.92	0.92	0.92

105

106 *b. GPM Microwave Imager*

107 Data from the GPM Microwave Imager (GMI) is utilized both in M2020 and in this study.  
108 GMI is a 13 channel conically scanning microwave radiometer aboard the Global  
109 Precipitation Measurement (GPM) Mission. Launched in February 2014, GPM is in a non-  
110 sun synchronous orbit with an inclination angle of  $65^\circ$ . The conical scan has a nominal Earth  
111 incidence angle of  $52.8^\circ$  for channels at or below 89 GHz and  $49.2^\circ$  for channels at or above  
112 166 GHz (Skofronick-Jackson et al., 2017; Petty and Bennartz, 2017). The conical scan  
113 geometry with a near constant Earth incidence angle/zenith viewing makes it possible for  
114 more accurate emissivity databases specifically designed for GMI as in M2020, given there is  
115 an Earth incidence angle dependence on emissivity. The channels for GMI are shown in  
116 Table 1, and range in frequency between 10.6-183 GHz. All 13 channels are sensitive to  
117 precipitation. The lower frequency channels (10.6-37 GHz) are most sensitive to emission  
118 from liquid precipitation, and higher frequencies (89-183GHz) are most sensitive to ice  
119 scattering. Channels 12 ( $183 \pm 3$  GHz V), and 13 ( $183 \pm 7$  GHz V) are strongly sensitive to  
120 water vapor and have a relatively weak surface sensitivity outside polar regions and high  
121 elevations (i.e., anywhere there is a low concentration of water vapor). Additionally, the  
122 presence of ice sheets in such regions enhance surface sensitivity. In the absence of scattering  
123 due to clouds and precipitation, Channel 5 (23 GHz) along with Channels 10-11 (166 GHz  
124 V/H) also have sensitivity to water vapor in addition to surface sensitivity, however, this  
125 sensitivity is weaker than the 183 GHz channels. Channels 10-11 are typically considered  
126 surface sensitive when column water vapor is approximately less than 20 mm (Munchak et  
127 al., 2020). Currently, in the GEOS-ADAS channels are only assimilated over water using 23  
128 GHz, 37 GHz V, 166 GHz V,  $183 \pm 3$  GHz V, and  $183 \pm 7$  GHz V (Kim et al., 2020). In  
129 future assimilation work over land snow and ice, a different channel selection may be  
130 necessary. Any remaining emissivity uncertainty may result in large uncertainty in  
131 brightness temperature simulation, which may conflate signals from different geophysical  
132 parameters.

### 133 *c. Emissivity from Active-Passive Microwave Land Surface Database*

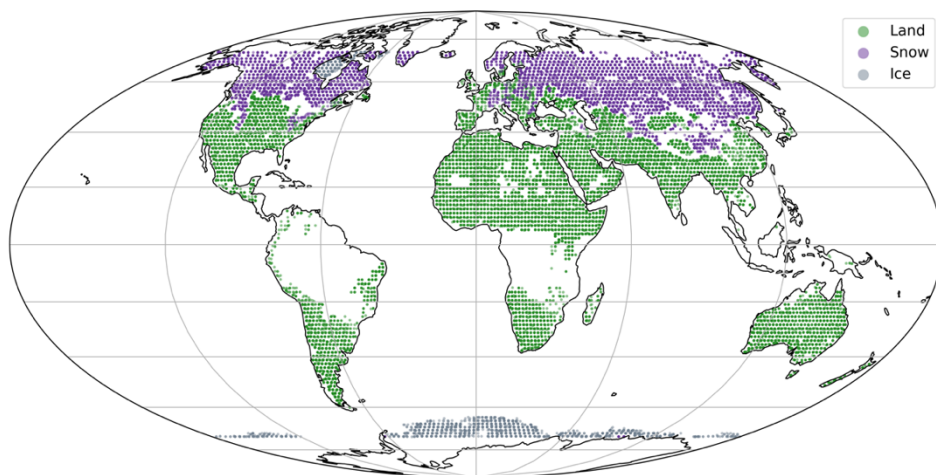
134 Recently, Munchak et al., 2020 presented an Active-Passive Microwave Land Surface  
135 Database that includes monthly average emissivity values for GMI Channels 1-11. The  
136 average emissivities were derived using 5 years of emissivity retrievals (March 2014-  
137 February 2019) using data from GPM, thus providing a climatological emissivity value on a  
138 monthly basis. The climatology is constructed taking each month of the year (January-  
139 December) and grouping the 5 years of retrievals by month. The data is provided using a 0.25

140 x 0.25 degree global (67S-67N) grid, with an average value of emissivity at each grid cell  
141 over land, snow, and ice (with a fill value for no retrieval). The dataset is unique in that it  
142 utilizes the DPR on GMI to both filter out precipitation-contaminated observations, along  
143 with retrieval diagnostics and ancillary data from MERRA-2 (Gelaro et al., 2017). The  
144 dataset also contains a surface classification based on the spectral emissivity and radar  
145 backscatter cross-section characteristics. The retrieval of emissivity uses GMI brightness  
146 temperatures taken from the Level -1CR data product, surface normalized radar cross section  
147 ( $\sigma_0$ ) from the DPR Level 2A data product, along with data from MERRA-2 which is used as  
148 the a-priori atmospheric profiles and surface temperature for the retrieval of emissivity from  
149 brightness temperatures.

150 Fig. 1 shows GMI observations simulated and compared in this study. It should be noted that  
151 there are no retrieved 166 GHz emissivities over portions of Africa and South America in the  
152 M2020 dataset due to insufficient sensitivity of this channel to the surface in these regions  
153 due to high water vapor amounts. To simplify the implementation, no GMI observations are  
154 considered over these regions (in white). The classification of land, snow and ice are taken  
155 from the GEOS Model surface type. The surface classification in GEOS is derived from the  
156 catchment based model of Koster et al. 2000 over land, the Multi-layer snow model of  
157 Steiglitz et al. 2001, and the Operational Sea Surface Temperature and Ice Analysis system  
158 (OSTIA; Donlon et al. 2012).

159

Observation Locations and Classification (Land, Snow, Ice)



160  
161 Fig. 1. Locations of all GMI observations over Land, Snow and Ice used in this study.  
162

### 163 **3. Evaluation of Active-Passive Microwave Land Surface Database using** 164 **GEOS**

165 In this work the emissivity models available in the GEOS-ADAS are compared against the  
166 climatological emissivity values available in M2020. GMI has 13 channels, with varied  
167 sensitivity to the surface. the two water vapor channels at 183 GHz having less surface  
168 sensitivity than others outside polar regions, or regions with ice sheets. Currently, the GEOS-  
169 ADAS only assimilates 23 GHz, 37 GHz V, 166 GHz V, and two vertically polarized water  
170 vapor channels at 183 GHz over ocean. No GMI radiances over land, snow and ice are used.  
171 This resulted in some slight modifications to the GEOS-ADAS along with some other quality  
172 control decisions. These are described in Section 3.1, and in Section 3.2 simulated GMI  
173 observations using the default GEOS-ADAS emissivity models are compared against that of  
174 M2020.

#### 175 *a. Evaluation method using the GEOS-ADAS*

176 The comparisons made in this study use two slightly modified versions of the GEOS-ADAS  
177 version 5.27.1. Most of the code changes are common among both systems. First, version  
178 5.27.1 of the GEOS-ADAS rejects GMI observations over land, snow, ice and mixed  
179 surfaces. This check is modified to only reject mixed surfaces for both cases. While having  
180 the ability to simulate mixed surfaces is desirable, as a first step to evaluate the emissivity  
181 database of M2020, it is best to compare surfaces without the complexity of accounting for  
182 surface cover fractions which may introduce more representativeness error. Next, a quality  
183 control check that rejects GMI observations north of 55 degrees latitude, and south of -55  
184 degrees latitude is removed. This check was originally added to the GEOS-ADAS to avoid  
185 sea ice. A goal of this study is to investigate the ice emissivity available in M2020 and  
186 compare it to the default values in CRTM for comparison, therefore, the latitude check is  
187 removed for both simulations. Finally, to avoid the complexities of comparing regions  
188 affected by rain or clouds a check is added to flag GMI observations with a total sum of ice  
189 and liquid water content of  $0.15 \text{ kg/m}^2$  and remove them from consideration.

190 For the case using M2020 there were a few steps necessary to ingest emissivity into the  
191 GEOS-ADAS. First, a netcdf file was generated based on data provided in M2020. The  
192 emissivity dataset is a 5-dimensional array indexed by channel, latitude, longitude, month,  
193 and surface type (land, snow, or sea ice). Each observation is interpolated using a nearest  
194 neighbor approach to the M2020 latitude and longitude grid. The month of the observation is  
195 used as an index along with the surface type given by the GEOS-ADAS. For the two 183

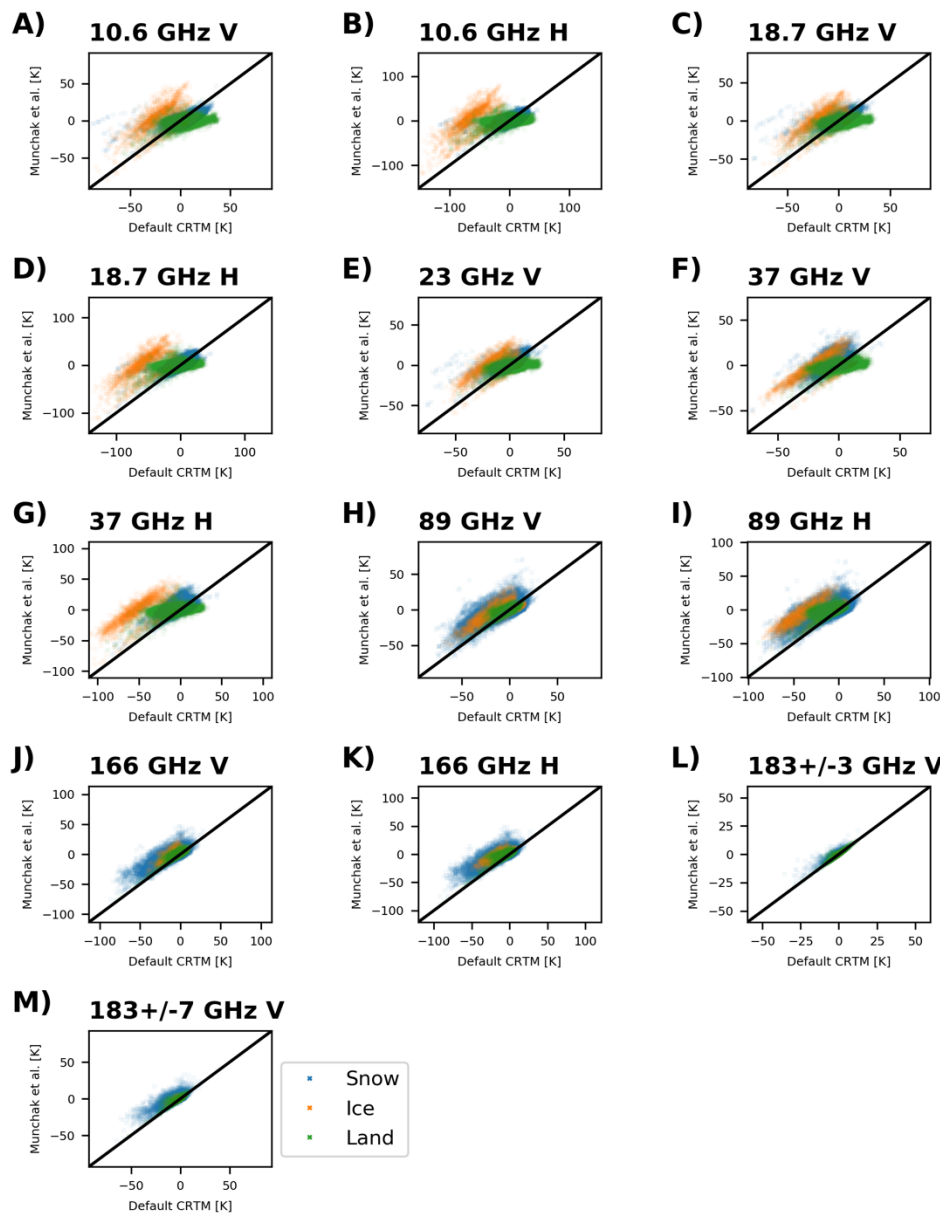
196 GHz channels, there are no retrieved values available from M2020. Instead, the emissivity  
197 values from the 166 GHz V channel are used to approximate the emissivity value. A similar  
198 assumption was made in Baordo and Geer 2016, using 89 GHz emissivity values to estimate  
199 183 GHz emissivity for the SSMIS instrument.

200 Radiative transfer calculations are performed by running the GSI in a standalone mode in  
201 place of a full 4D-EnVar experiment. In standalone mode, the background fields are taken  
202 from an existing run of the GEOS-ADAS. The run is an experimental version of the GEOS-  
203 Forward Processing system using the version 5.27.1 of the GEOS-ADAS which assimilates  
204 the full suite of Infrared, Microwave, and conventional observations including an all-sky  
205 assimilation of GMI over ocean surfaces. This allows a quick method to produce simulated  
206 observations that are effectively offline simulations for comparison of the emissivity models,  
207 and since the background fields are constant in the comparisons, the only differences are due  
208 to the changes in emissivity in the radiative transfer calculations. The background fields are  
209 on hourly intervals and are interpolated in space and time to the observation location. One  
210 week of GMI observations are simulated for December 1, 2020 through December 7, 2020  
211 for four synoptic time windows at 6 hour intervals. In all comparisons to follow the  
212 observation minus background values are used to indicate whether the emissivity model  
213 improves the simulation. A smaller magnitude (absolute value) observation minus  
214 background indicates the simulation is closer, and therefore considered an improvement. In  
215 all comparisons, no bias correction is applied to the simulated values.

#### 216 *b. Results of Evaluation*

217 The simulated brightness temperatures (also commonly referred to as the background) using  
218 M2020 and using the default CRTM are compared against GMI observations for the first  
219 week of December 2020. In Fig. 2, scatter plots observation minus background (OMB) are  
220 shown for the 13 GMI channels. One feature that clearly stands out is ice (in orange) and  
221 snow surfaces (in blue) exhibit the largest scatter in OMB values in both in the M2020  
222 simulation and default CRTM simulation relative to Land (in green). Next, departures over  
223 land are significantly smaller for M2020 in panels A-G. Similarly, large departures of OMBs  
224 over ice are reduced by using M2020 in place of the default CRTM value of 0.92 emissivity.  
225 This is especially true for horizontal polarization channels (shown in Fig 2. panels B, D, G,  
226 D). Finally, it is clear the default CRTM exhibits a bias over ice in panels A-I and over snow  
227 in panels H-M (values not centered around zero), whereas in the M2020 simulation the values

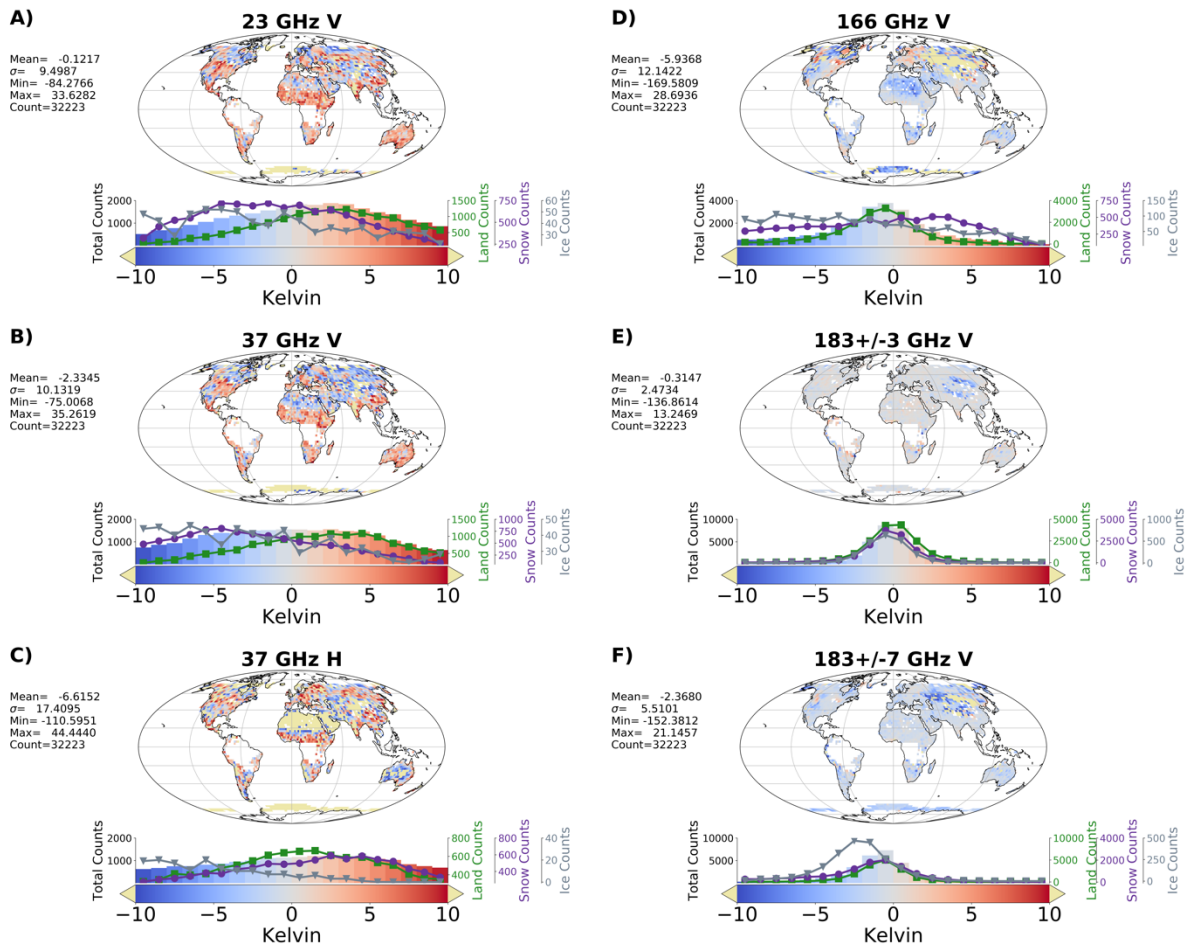
228 are closely centered around zero. For reference, all observation points and their classification  
 229 as either over land, snow or ice are shown in Fig. 1.



230  
 231 Fig. 2. Scatter plots of GEOS-ADAS calculated values of observation minus background  
 232 using Munchak et al., 2020 vs default CRTM values.  
 233

234 Next, OMB values are averaged spatially on a 2.5 x 2.5 degree averaging grid over the week  
 235 and plotted spatially, while all observation locations are used to compute histograms in Figs.  
 236 3 and 4. In each panel, the 2D map plot in the upper part shows the averaged OMB at each

237 grid box, and the plot in the lower part displays histograms for all data (shaded area), data  
238 over land (green line with squares), over ice (gray line with triangle), and over snow (purple  
239 line with circle), respectively. In lieu of plotting all GMI channels, only channels currently  
240 assimilated operationally over ocean in the GEOS-ADAS are plotted in Figs 3-4. The  
241 remaining channels are plotted for reference in Appendix A. Significant improvements can be  
242 observed in Fig. 4 (M2020 simulation) vs Fig. 3 (CRTM default) spatially. First, there are far  
243 fewer points in yellow indicating values outside the +/- 10 K range. Next, there are many  
244 more regions that are in the +/- 5K OMB range in Fig. 4 vs Fig. 3. Moreover, when CRTM  
245 default emissivities are used, the OMB values of the channels with horizontal polarization are  
246 much worse than those vertical polarization; but when M2020 emissivities are used, the OMB  
247 differences between horizontal and vertical polarization are decreased. These results are in  
248 agreement with those observed in Fig. 2. Additionally, there are some regional improvements  
249 that can be seen comparing Figs 3-4. Simulated brightness temperatures are much closer to  
250 observed brightness temperatures at 23 GHz and 37 GHz (V/H) in North Africa comparing  
251 Fig 3 to Fig 4 (Panels A-C). Regions over ice show an improvement over regions near  
252 Antarctica in Fig. 4 vs Fig. 3. For the 23 GHz and 37 GHz (V/H) channels, large regions  
253 exceeding 10 K departures are reduced around Antarctica, along with departures closer to  
254 zero for the 183 GHz channels. In Northern Asia, snow covered regions show improvements  
255 most clearly comparing Fig. 3 and 4 for the 166 GHz and 183 GHz channels where  
256 departures are closer to zero.

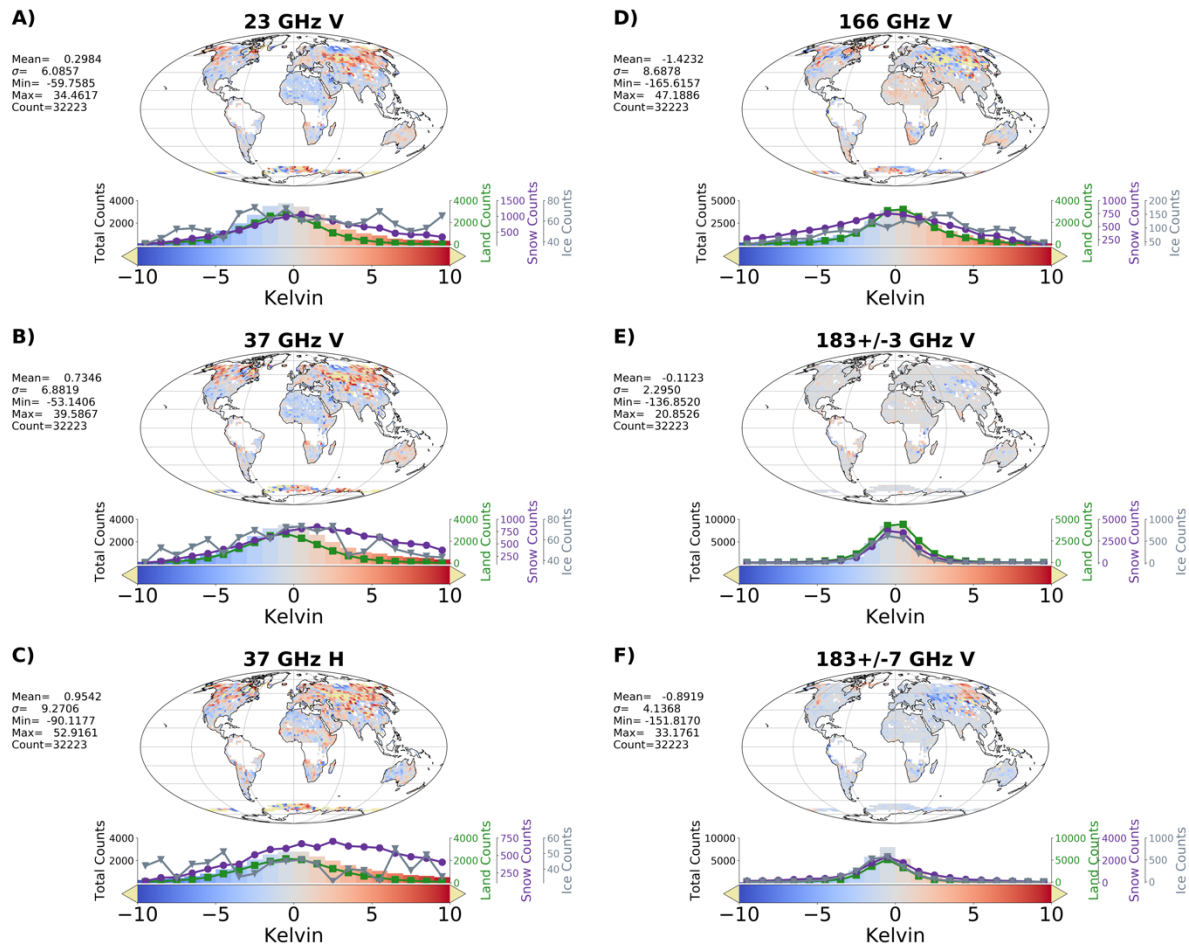


257

258

259

Fig. 3. GEOS-ADAS calculated values of observation minus background using default CRTM values.



260

261 Fig. 4. GEOS-ADAS calculated values of observation minus background using Munchak  
 262 et al., 2020.

263

264 Observing the histograms of OMB values in Figs. 3-4, in Fig. 4 there is a clear gaussian  
 265 pattern nearly centered around zero for all channels. Fig. 3 only has a gaussian pattern for

266 frequencies at 166 GHz and above (Panels D-F). The two 183 GHz channels have little

267 sensitivity to surface, especially the +/- 3 GHz channel which has a sensitivity which peaks

268 higher in the atmosphere. The improvements are further shown in Fig. 5 which contains

269 spatial plots and histograms of the difference between the absolute values of OMB

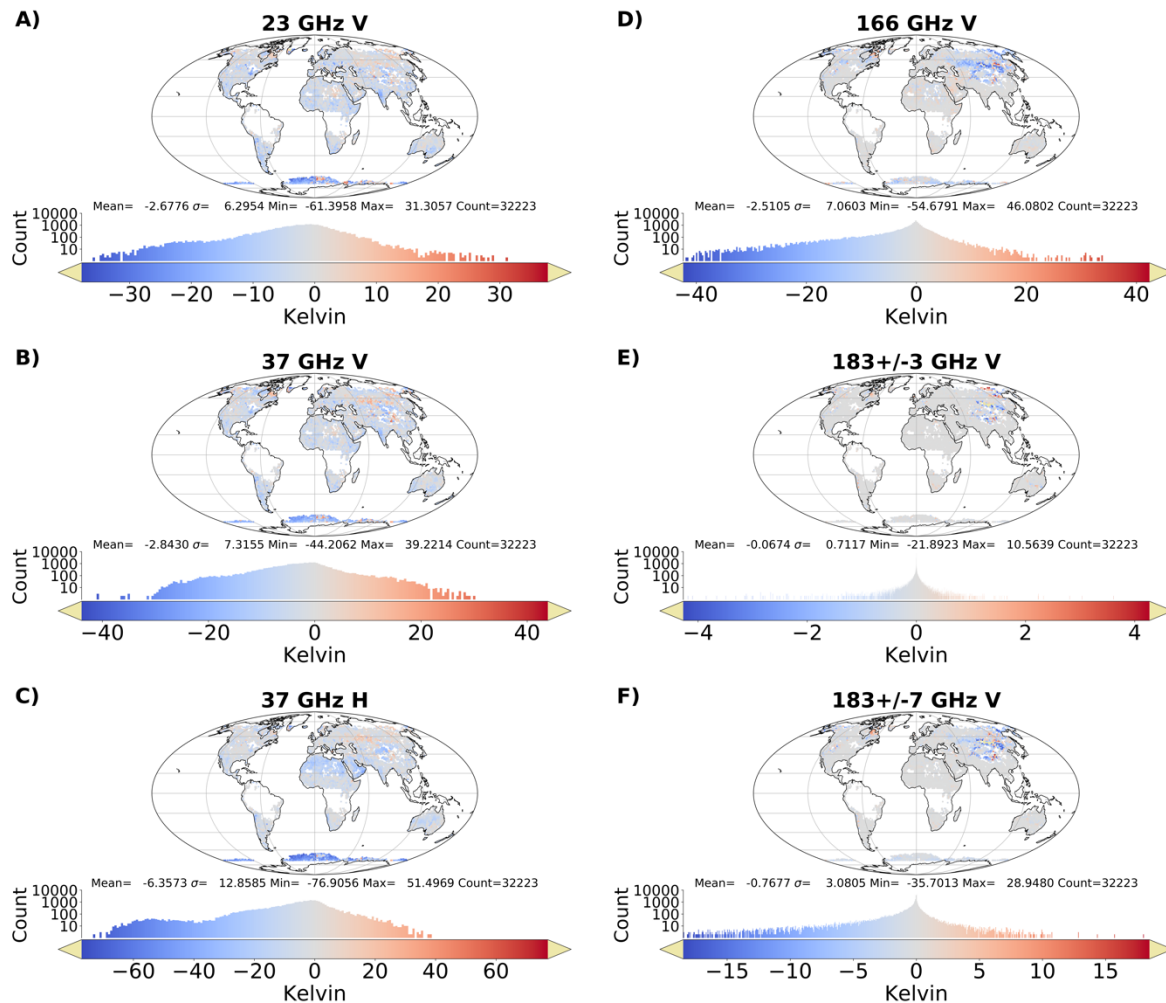
270 simulations using M2020 minus the absolute values of OMB using the default CRTM.

271 Negative values indicate the M2020 simulation is closer to the observation (blue), positive

272 values (red) indicate it is further away from the observation. Overall, with exception to the

273 183 GHz +/-3 channel (Panel E), there are many points where the OMB indicates the M2020

274 simulation is closer to the observation.



275

276 Fig. 5. Difference in GEOS-ADAS calculated absolute values of observation minus  
 277 background using Munchak et al., 2020 minus values calculated with default CRTM.

278

279 Next, the relative improvement over land, snow, and ice are considered. Comparing both  
 280 spatially and viewing histograms in Figs. 1, 3 and 4, there are clear improvements over land.  
 281 Comparing the histograms over land (green squares), there is a clear gaussian pattern with a  
 282 nearly centered around zero for all channels for M2020 (Fig. 4), whereas in Fig. 3 there are  
 283 cases where there is a gaussian pattern for the default CRTM case, however, for all channels  
 284 there is an improvement for the M2020 case (Fig. 4). For points identified as snow covered  
 285 for the default CRTM and M2020 simulations in Figs. 3-4, improvements are still noticeable,  
 286 they are far less dramatic with long tails remaining in the distribution for Fig. 4. Comparing  
 287 histograms and spatial distributions of OMB over ice in Figs. 3-4, there are improvements,  
 288 however, the improvements are not as dramatic as either over land or snow. One notable  
 289 exception is for the 183 +/- 7 GHz channel when comparing Fig 3-4 panel F, the grey  
 290 histograms (indicating observations over ice) have a gaussian pattern more closely centered  
 291 around zero in Fig.4 indicating simulations using M2020 are closer to the GMI observations.

292 Improvements relative to the default CRTM configuration over ice are somewhat expected,  
293 especially for channels over ice which utilize a default value of 0.92 by default in CRTM vs  
294 using the emissivity provided by M2020. Similar expectations would apply to frequencies of  
295 89 GHz and above where only constant values of emissivity are used over land and snow  
296 surfaces (see Table 1). Improvements relative to the default CRTM configuration over land  
297 and snow below 89 GHz indicate that the LandEm of Weng et al. 2001 does not perform as  
298 well as M2020.

299

#### 300 **4. Summary and Future Work**

301 In this work it has been shown that using emissivity values from M2020 can improve  
302 simulation of brightness temperatures from GMI using the GEOS-ADAS. The improvements  
303 are most noticeable over land with a dramatic improvement, followed by snow and ice with a  
304 less dramatic improvement. With such a dramatic improvement over land, it may be possible  
305 to attempt assimilating surface sensitive GMI channels over land, or at the very least as a first  
306 guess for an in-line retrieval or adding emissivity to the GEOS-ADAS control vector. This  
307 may be necessary given M2020 is a climatology, and variations in surface properties such as  
308 soil moisture may result in significant departures especially at lower frequency channels.  
309 Assimilating surface sensitive channels over land could provide information regarding  
310 temperature and moisture in the Planetary Boundary Layer in the GEOS-ADAS. This was  
311 noted as a key need by the decadal survey (NASEM, 2018), and is an on-going effort at the  
312 Global Modeling and Assimilation Office. Additionally, it may be possible to utilize M2020  
313 for similar sensors such as AMSR-2 which has an Earth incidence angle of 55° (Maeda et al.,  
314 2016), however, this would require rigorous testing. Full observing system experiments will  
315 be conducted using surface sensitive channels over land, snow and sea ice which could  
316 provide more data in the planetary boundary layer, thus improving its representation in the  
317 GEOS system.

#### 318 *Acknowledgments.*

319 The authors would like to thank the NASA GSFC Science Task Group (STG) on  
320 “Evaluation and Improvement of Surface Emissivity for Enhanced Earth and Planetary  
321 Remote Sensing” for support, and funding to conduct this study.

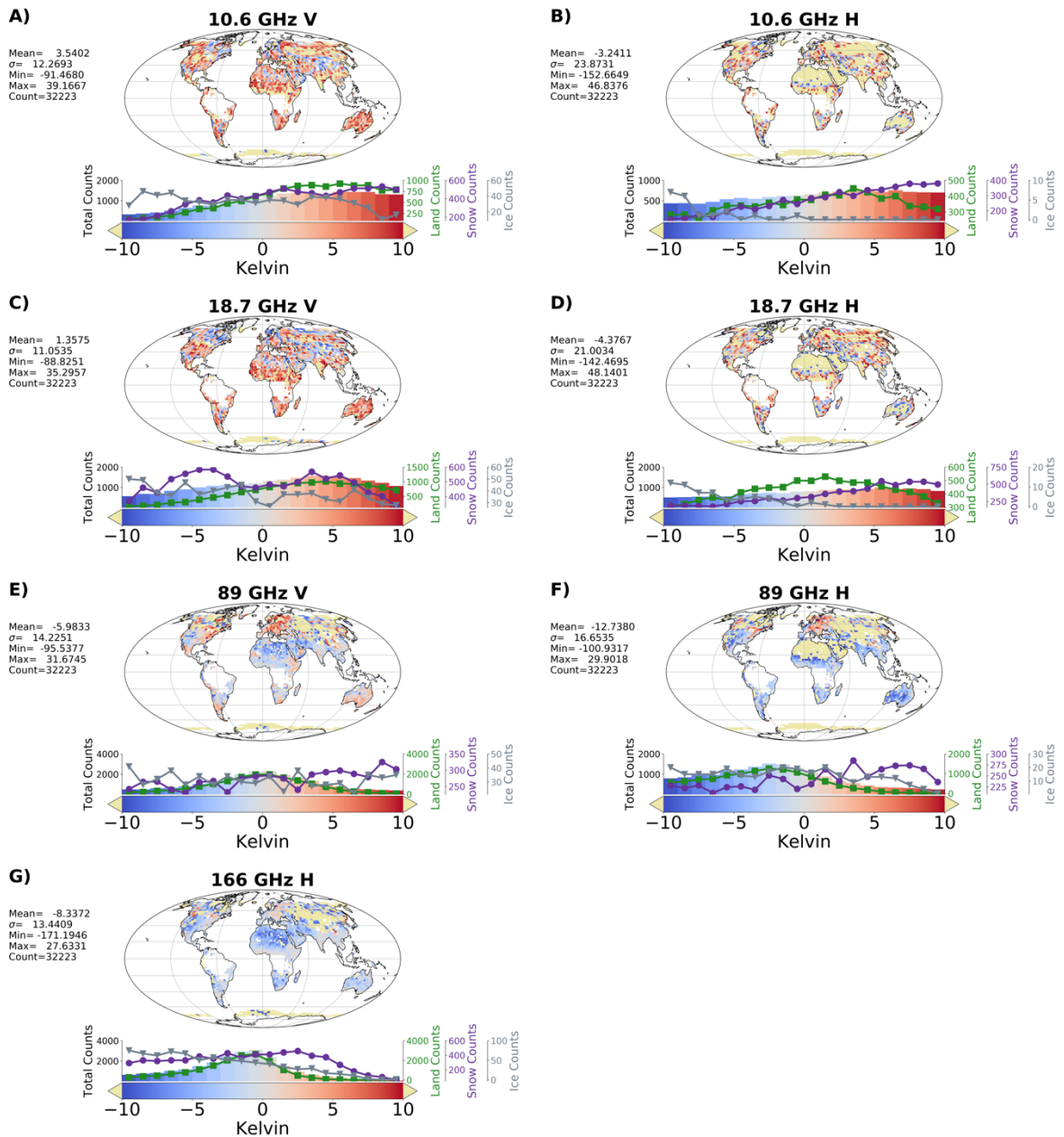
322

#### 323 *Data Availability Statement.*

324 Data used for this study includes L1C calibrated brightness temperatures freely available  
325 from <https://doi.org/10.5067/GPM/GMI/GPM/1C/05>. Data from Munchak et al., 2020 is  
326 available from <https://dx.doi.org/10.21227/fypd-zj65>.  
327

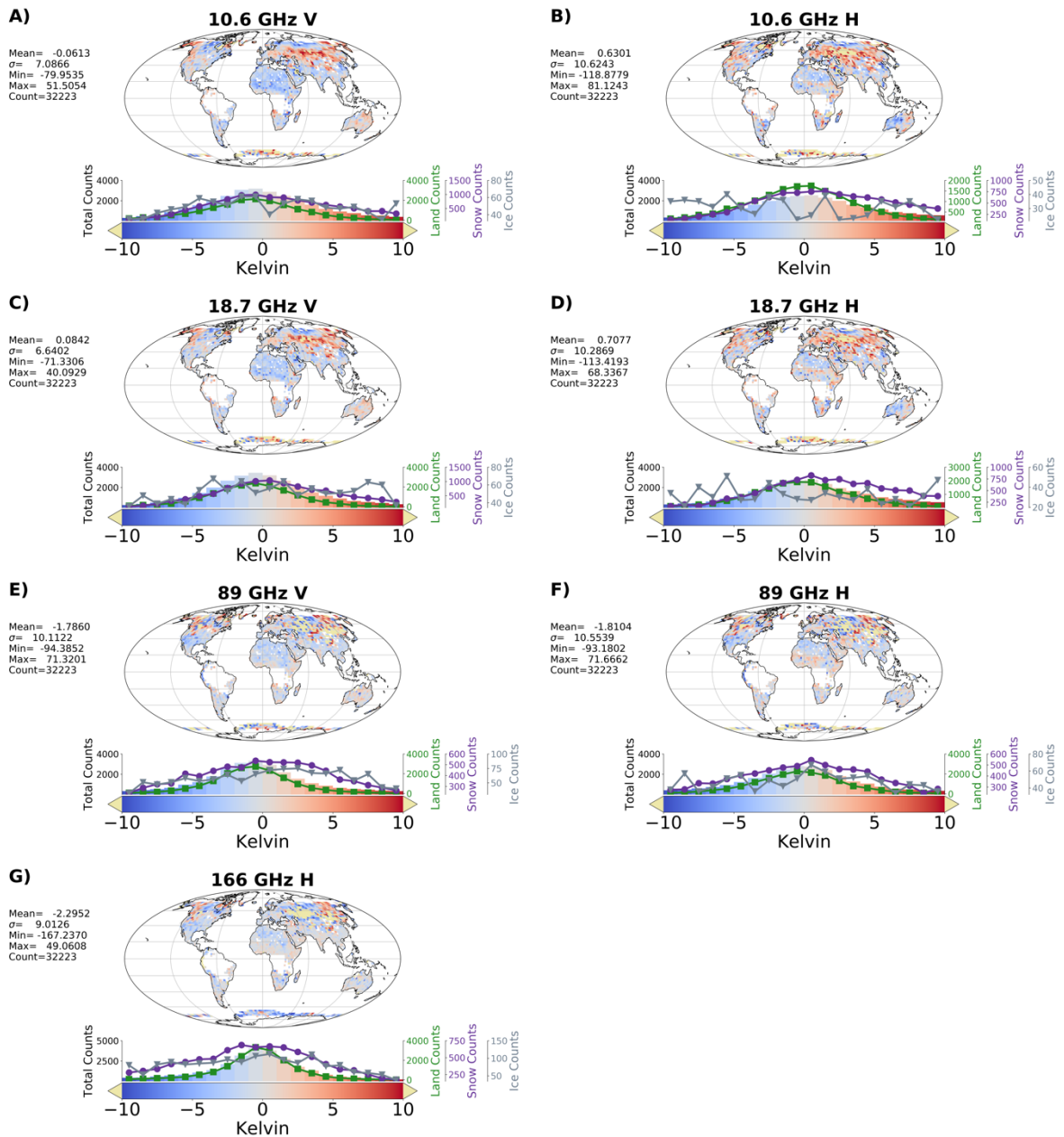
## 328 **Appendix A – Spatial differences for Additional Channels**

329 In section 3b Figs. 3-5 were introduced to highlight differences between using the default  
330 emissivity model present in CRTM and simulations performed using CRTM with the M2020  
331 emissivity database. To simplify the discussion, only channels currently assimilated over  
332 ocean in the GEOS-ADAS were included. Other centers may have different channel  
333 selections, thus the remaining channels for GMI are plotted following Figs 3-5 in Figs A1-  
334 A3.



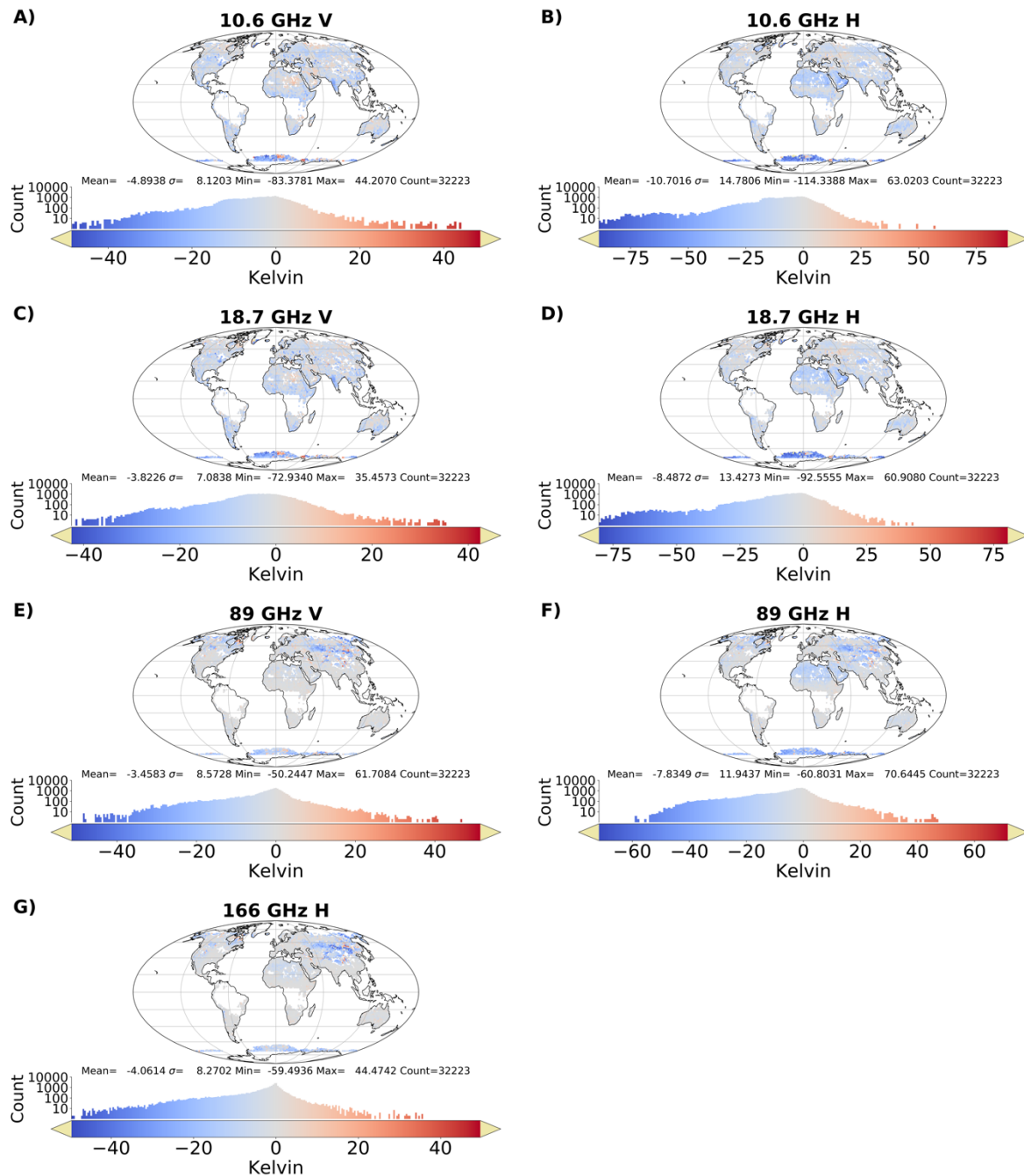
335  
 336  
 337

Fig A1. GEOS-ADAS calculated values of observation minus background using default CRTM values following Fig 3.



338  
 339  
 340

Fig A2. GEOS-ADAS calculated values of observation minus background using Munchak et al., 2020 following Fig 4.



341  
 342 Fig A3. . Difference in GEOS-ADAS calculated absolute values of observation minus  
 343 background using Munchak et al., 2020 minus values calculated with default CRTM,  
 344 following Fig 5.  
 345  
 346

347 REFERENCES

348 Baordo, F., and A. J. Geer, 2016: Assimilation of SSMIS humidity-sounding channels in all-  
 349 sky conditions over land using a dynamic emissivity retrieval. *Quarterly Journal of the*  
 350 *Royal Meteorological Society*, **142**, 2854–2866, <https://doi.org/10.1002/qj.2873>.  
 351 Chen, M., and F. Weng, 2016: Modeling land surface roughness effect on soil microwave  
 352 emission in community surface emissivity model. *IEEE Transactions on Geoscience*  
 353 *and Remote Sensing*, **54**, 1716–1726, <https://doi.org/10.1109/TGRS.2015.2487885>.

354 Chen, Y., F. Weng, Y. Han, and Q. Liu, 2009: Validation of the community radiative transfer  
355 model by using cloudsat data. *Journal of Geophysical Research Atmospheres*, **114**,  
356 <https://doi.org/10.1029/2007JD009561>.

357 Donlon, C. J., M. Martin, J. Stark, J. Roberts-Jones, E. Fiedler, and W. Wimmer, 2012: The  
358 Operational Sea Surface Temperature and Sea Ice Analysis (OSTIA) system. *Remote*  
359 *Sensing of Environment*, **116**, 140–158, <https://doi.org/10.1016/j.rse.2010.10.017>.

360 Gelaro, R., and Coauthors, 2017: The modern-era retrospective analysis for research and  
361 applications, version 2 (MERRA-2). *Journal of Climate*, **30**, 5419–5454,  
362 <https://doi.org/10.1175/JCLI-D-16-0758.1>.

363 Han, Y., P. van Delst, Q. Liu, F. Weng, B. Yan, R. Treadon, and J. Derber, 2006: *JCSDA*  
364 *Community Radiative Transfer Model (CRTM)-Version 1*.

365 Kim, M. J., J. Jin, A. E. L. Akkraoui, W. McCarty, R. Todling, G. U. Wei, and R. Gelaro,  
366 2020: The framework for assimilating all-sky GPM microwave imager brightness  
367 temperature data in the NASA GEOS data assimilation system. *Monthly Weather*  
368 *Review*, **48**, 2433–2455, <https://doi.org/10.1175/MWR-D-19-0100.1>.

369 Koster, R. D., M. J. Suarez, A. Ducharne, M. Stieglitz, and P. Kumar, 2000: A catchment-  
370 based approach to modeling land surface processes in a general circulation model 1.  
371 Model structure. *Journal of Geophysical Research Atmospheres*, **105**, 24809–24822,  
372 <https://doi.org/10.1029/2000JD900327>.

373 Maeda, T., Y. Taniguchi, and K. Imaoka, 2016: GCOM-W1 AMSR2 Level 1R Product:  
374 Dataset of Brightness Temperature Modified Using the Antenna Pattern Matching  
375 Technique. *IEEE Transactions on Geoscience and Remote Sensing*, **54**, 770–782,  
376 <https://doi.org/10.1109/TGRS.2015.2465170>.

377 Mätzer, C., 1994: Passive Microwave Signatures of Landscapes in Winter. *Meteorol. Atmos.*  
378 *Phys*, **54**, 241–260.

379 Munchak, S. J., S. Ringerud, L. Brucker, Y. You, I. de Gelis, and C. Prigent, 2020: An  
380 Active-Passive Microwave Land Surface Database from GPM. *IEEE Transactions on*  
381 *Geoscience and Remote Sensing*, **58**, 6224–6242,  
382 <https://doi.org/10.1109/TGRS.2020.2975477>.

383 National Academies of Sciences Engineering and Medicine (NASSEM), 2018: Thriving on  
384 Our Changing Planet: A Decadal Strategy for Earth Observation from Space. The  
385 National Academies Press. Washington, DC, doi: 10.17226/24938.

386 Petty, G. W., and R. Bennartz, 2017: Field-of-view characteristics and resolution matching  
387 for the Global Precipitation Measurement (GPM) Microwave Imager (GMI).  
388 *Atmospheric Measurement Techniques*, **10**, 745–758, [https://doi.org/10.5194/amt-10-](https://doi.org/10.5194/amt-10-745-2017)  
389 [745-2017](https://doi.org/10.5194/amt-10-745-2017).

390 Saunders, R., and Coauthors, 2020: *RTTOV-13 Science and Validation Report RTTOV-13*. 1–  
391 106 pp.

392 Skofronick-Jackson, G., and Coauthors, 2017: The global precipitation measurement (GPM)  
393 mission for science and Society. *Bulletin of the American Meteorological Society*, **98**,  
394 1679–1695, <https://doi.org/10.1175/BAMS-D-15-00306.1>.

395 Stieglitz, M., A. Ducharne, R. Koster, and M. Suarez, 2001: The Impact of Detailed Snow  
396 Physics on the Simulation of Snow Cover and Subsurface Thermodynamics at  
397 Continental Scales. *Journal of Hydrometeorology*, **2**, 228–242,  
398 [https://doi.org/10.1175/1525-7541\(2001\)002<0228:TIODSP>2.0.CO;2](https://doi.org/10.1175/1525-7541(2001)002<0228:TIODSP>2.0.CO;2).

399 Todling, R., and A. El Akkraoui, 2018: The GMAO hybrid ensemble-variational atmospheric  
400 data assimilation system: Version 2.0. NASA/TM-2018-104606, Vol. 50, 184 pp.

401 Wang, D., and Coauthors, 2017: Surface emissivity at microwaves to millimeter waves over  
402 polar regions: Parameterization and evaluation with aircraft experiments. *Journal of*

403        *Atmospheric and Oceanic Technology*, **34**, 1039–1059, <https://doi.org/10.1175/JTECH->  
404        D-16-0188.1.  
405        Weng, F., B. Yan, and N. C. Grody, 2001: A microwave land emissivity model. *Journal of*  
406        *Geophysical Research Atmospheres*, **106**, 20115–20123,  
407        <https://doi.org/10.1029/2001JD900019>.  
408        Zhu, Y., R. Todling, and J. Jin, 2021: Improving the use of surface-sensitive radiances in the  
409        GMAO GEOS system. *The 23rd International TOVS Study Conference*,  
410        <http://cimss.ssec.wisc.edu/itwg/itsc/itsc23/agendas/posters/poster.2p.20.zhu.pdf>  
411